Elkady, Mustafa, Elmarakbi, Ahmed and MacIntyre, John (2012) Enhancement of Vehicle Safety and Improving Vehicle Yaw Behaviour Due to Offset Collisions Using Vehicle Dynamics. International Journal of Vehicle Safety, 6 (2). pp. 110-133. ISSN 1479-3105

Downloaded from: http://sure.sunderland.ac.uk/id/eprint/3140/

Usage guidelines

Please refer to the usage guidelines at http://sure.sunderland.ac.uk/policies.html or alternatively contact sure@sunderland.ac.uk.

Enhancement of vehicle safety and improving vehicle yaw behaviour due to offset collision using vehicle dynamics

Mustafa Elkady*

Department of Computing, Engineering and Technology,
University of Sunderland,
The Sir Tom Cowie Campus at St Peter's,
St Peter's Way, Sunderland, SR6 0DD, UK
and
Department of Automotive Engineering,
Ain Shams University, Cairo, Egypt
Email: mustafa.elkady@research.sunderland.ac.uk
*Corresponding author

Ahmed Elmarakbi and
John MacIntyre

Department of Computing, Engineering and Technology,
University of Sunderland,
The Sir Tom Cowie Campus at St Peter's,
St Peter's Way, Sunderland, SR6 0DD, UK
Email: ahmed.elmarakbi@sunderland.ac.uk
Email: john.macintyre@sunderland.ac.uk

Abstract: This study aims to optimise Vehicle Dynamic Control Systems (VDCS) in offset impact for vehicle collision mitigation. A proposed unique 3-D full-car mathematical model is developed and solved numerically to carry out this analysis. In this model, vehicle dynamics is studied together with the vehicle crash structural dynamics. Validation of the vehicle crash structure of the proposed model is achieved to ensure that the modelling of the crumple zone and the dynamic responses are reliable. It is demonstrated from the numerical simulations that the vehicle dynamic responses are captured and analysed and the influence of VDCS is determined accurately. In addition, it is shown that the mathematical model is flexible, useful and can be used in optimisation studies.

Keywords: active safety; collision mitigation; vehicle dynamics; vehicle control; mathematical modelling; numerical simulations.

Reference to this paper should be made as follows: Elkady, M., Elmarakbi, A. and MacIntyre, J. (2012) 'Enhancement of vehicle safety and improving vehicle yaw behaviour due to offset collision using vehicle dynamics', *Int. J. Vehicle Safety*, Vol. 6, No. 2, pp.110–133.

Copyright © 2012 Inderscience Enterprises Ltd.

1 Introduction

There has been much research into Vehicle Dynamic Control Systems (VDCS) in order to improve the vehicle stability, safety and ride characteristics. In case of vehicle stability, the Anti-Lock Braking System (ABS) and the yaw moment control system are used to help vehicle stability during emergency manoeuvres. While the ABS also helps in reducing the vehicle stopping distance, the active suspension (AS) control system integrated with the ABS was used for more reduction of the vehicle stopping distance to improve the vehicle safety (Alleyne, 1997; Ting and Lin, 2004). On the other hand, seat belts, air bags and Advanced Driver Assistance Systems (ADAS) were developed to mitigate vehicle collision when a crash occurs. In addition, the front and side structures of vehicles are continuously being redesigned to improve crash energy absorption.

With regard to vehicle collision avoidance or mitigation, ADAS has been developed to prevent or decrease the likelihood of a crash during a collision (Seiler et al., 1998; Tamura et al., 2001; Jansson et al., 2002; Schoeneburg and Breitling, 2005; Gietelink et al., 2006). However, ADAS has yet to achieve its goal of preventing vehicle collision due to human factors, slow response actuators, uncertainty measurements and insufficient real tests. With respect to crash energy absorption, the frontal structure of a vehicle was optimised to absorb more crash energy and reduce the vehicle deceleration during crash. A frontal structure consisting of two special longitudinal members was discussed by Witteman and Kriens (1998). These members combine higher bending resistance characteristics without increasing axial stiffness. The longitudinal members integrated with a progressive folding pattern were used (Witteman, 1999) and a new multi-cell structure was proposed (Kim, 2002) in the design of a new frontal vehicle structure that can absorb more crash energy than conventional structures. In the same manner, two types of smart front-end structures were proposed to mitigate vehicle frontal collision (Elmarakbi and Zu, 2004); they consist of two hydraulic cylinders integrated with the front-end longitudinal members of conventional vehicles. The cited studies claimed that the vehicle front-end intrusions and vehicle body decelerations can be reduced.

In the area of investigation of the effect of the VDCS on vehicle collision, very little research has been carried out. The influence of the braking force on vehicle impact dynamics in low-speed rear-end collisions was studied by Mastandrea and Vangi (2005). It was confirmed that the braking force was not negligible in high-quality simulations of vehicle impact dynamics at low speed. The effect of vehicle braking, anti-pitch control system and Direct Yaw Control (DYC) on vehicle crash routine was investigated using ADAMS multi-body dynamics model (Hogan, 2008). Hogan's study found that the ABS has a harmful effect on vehicle crash performance during offset barrier impacts while DYC systems proved to significantly improve vehicle-to-vehicle collision. However, he mentioned that more research in the effect of VDCS on vehicle collision mitigation is recommended.

In this research, a new 6-Degree-of-Freedom (6-DOF) vehicle dynamics/ crash mathematical model has been developed to study the effect of VDCS on vehicle collision mitigation in offset frontal collision. The ABS and the AS control system are co-simulated with the mathematical model and are used to mitigate vehicle collision and reduce the vehicle body pitch angle, pitch acceleration, maximum yaw angle and yaw acceleration. Different scenarios of VDCS are studied to evaluate the optimum setting of VDCS for impending collision. In addition, the effect of the damping coefficient of the suspension system on vehicle crash is discussed.

2 The 6-DOF vehicle dynamics/crash mathematical model

Using mathematical models in crash simulations is useful at the first-design concept, because rapid analysis is required in this stage. In addition, the well-known advantage of mathematical modelling provides a quick simulation analysis compared with finite element models.

Vehicle crash structures are designed to be able to absorb the crash energy and control vehicle deformations; therefore, simple mathematical models are used to represent the vehicle front structure (Emori, 1968). In this model, vehicle mass is represented by lumped mass and vehicle structure is represented by a spring in a simple model to simulate frontal and rear-end vehicle collision processes. Also, other analyses and simulations of vehicle-to-barrier impact using a simple mass spring model were established by Kamal (1970). Kamal's study demonstrated that mathematical modelling can be accurately used for unlimited numbers of vehicle-to-barrier crash tests. To achieve enhanced occupant safety, the crash energy management system was investigated by Khattab (2010). This study, using a simple lumped-parameter model, discussed the applicability of providing variable energy absorbing properties as a function of the impact speed.

In this paper, a 6-DOF vehicle dynamics/crash mathematical model has been developed to optimise the VDCS in impending impact at offset crash scenarios for vehicle collision mitigation. The ABS, the DYC and the AS control systems are co-simulated with a four-wheel vehicle dynamic model and integrated with a non-linear front-end structure model as shown in Figure 1.

Figure 1 6-DOF vehicle dynamics/crash mathematical model

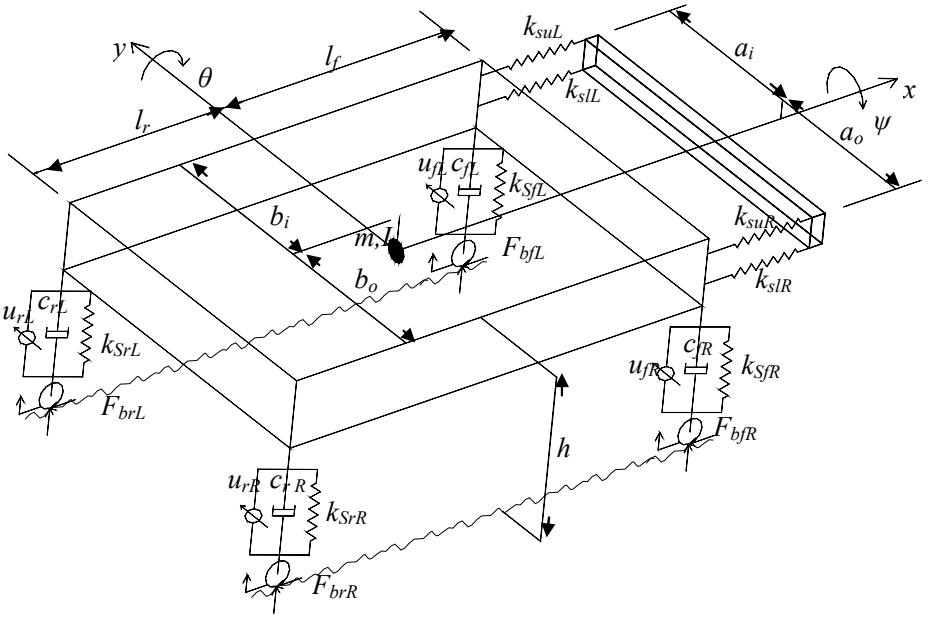

In Figure 1 l_f, l_r, l and h represent the longitudinal distance between the vehicle centre of gravity (CG) and front wheels; the longitudinal distance between the CG and rear wheels; the wheel base and the CG height, respectively. a_i and a_o are the distance between the point of impact and impacted springs and the distance between the point of impact and non-impacted springs, respectively. b_o and b_i are the distance between the CG and right wheels, the CG and left wheels, respectively. The other symbols in Figure 1 will be described in the following sections with the model equations.

Figures 2 and 3 are the pitch-plane and yaw-plane of the mathematical model, which are used to clarify and simplify the 3-D drawing. Figures 4 and 5 show the deformation of the front-end and vehicle pitching at the early stage and at the end of impact. At the first stage of impact, deformation of the front-end and vehicle pitching are small; while at the end of impact the deformation of the front-end reaches its maximum deformation; vehicle pitch angle increases, and the rear wheels leave the ground. It is assumed that the front-end springs are still horizontal during impact and they will not incline with the vehicle body.

Figure 2 Pitch-plane view and its free-body diagram (see online version for colours)

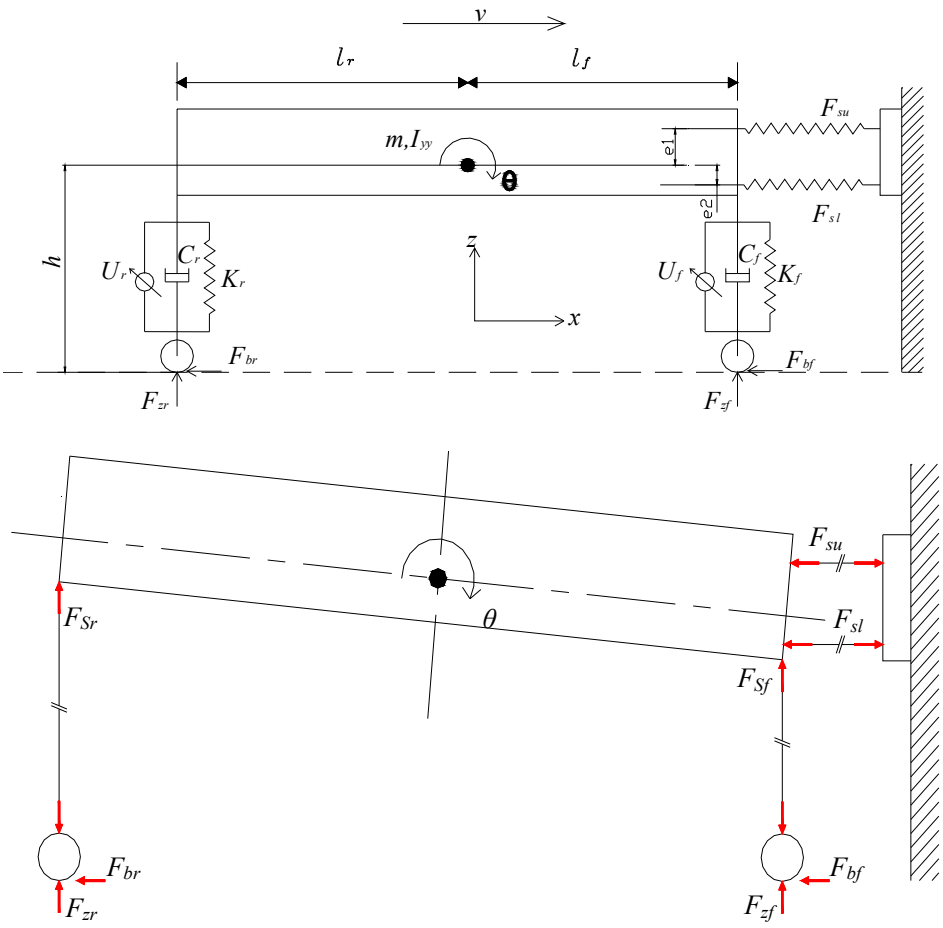

Figure 3 Yaw-plane view

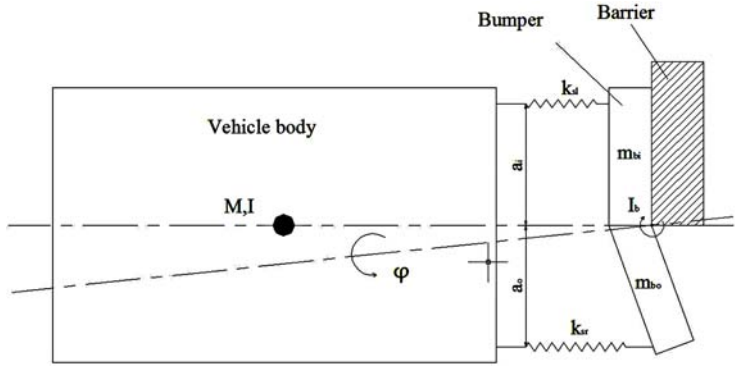

Figure 4 The mathematical model at the early stage of the impact

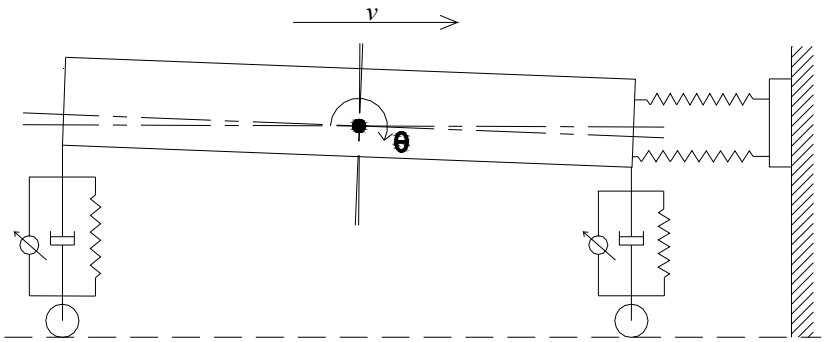

Figure 5 The mathematical model at the end of the impact

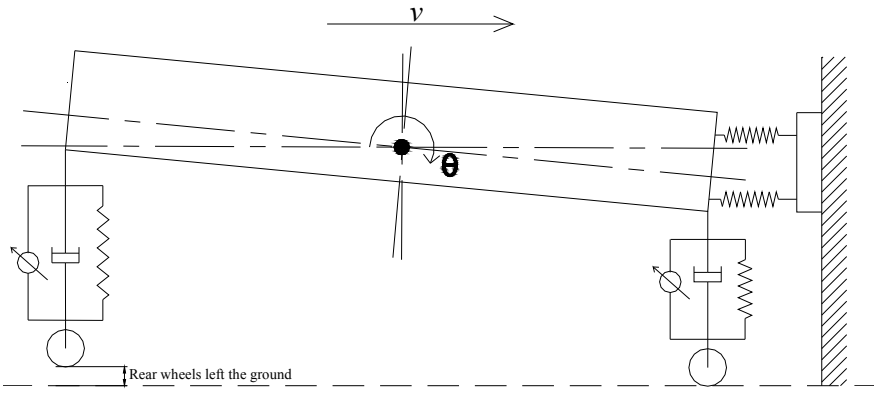

In this model, the vehicle body is represented by lumped mass *m* and four spring/damper units are used to represent the vehicle suspension system. Four non-linear springs are also proposed to represent the upper and lower members of the vehicle frontal structure. The mass of the impacted part of the bumper is neglected because it is not moving during

collision; while the mass of the rotational part of the bumper is considered. It is assumed that the vehicle moves on a flat asphalted road, thus neglecting the vertical movement of the tyres and road vertical forces. The vehicle body is pitching due to vehicle braking, the different values between the upper and lower crash forces, and the different distances between upper and lower members from the vehicle's centre of gravity.

3 Equation of motion of the mathematical model

In this section, the mathematical model and its equations of motion are developed to study and predict the dynamic response of the primary impact in offset vehicle-to-barrier crash scenarios. A finite element model (Figure 7) has been used to predict the attitude of the impacted side rail behaviour. It can be observed from the figure that the left bumper beam is inclined with the vehicle body, so it is assumed that the left spring will be inclined in the mathematical model, as shown in Figures 8 and 9. The model is a 6-DOF system, and its equations of motion can be written using Figures 1, 6 and 9 as:

$$m \cdot \ddot{x} + (F_{suR} + F_{slR}) \cdot \cos\gamma + (F_{suL} + F_{slL}) \cdot \cos\varphi + F_{bfR} + F_{bfL} + F_{brR} + F_{brL} = 0 \tag{1}$$

$$m \cdot \ddot{z} + F_{SfR} + F_{SfL} + F_{SrR} + F_{SrL} = 0 \tag{2}$$

$$\begin{aligned} &I_{yy} \cdot \ddot{\theta} - (F_{SfR} + F_{SfL}) \cdot l_f + (F_{SrR} + F_{SrL}) \cdot l_r + (F_{suR} \cdot \cos\gamma + F_{suL} \cdot \cos\varphi) \cdot d_1 \\ &-(F_{slR} \cdot \cos\gamma + F_{slL} \cdot \cos\varphi) \cdot d_2 - (F_{bfR} + F_{bfL} + F_{brR} + F_{brL}) \cdot (z + h) = 0 \end{aligned} \tag{3}$$

$$\begin{aligned} &I_{zz} \cdot \ddot{\varphi} + (F_{suR} + F_{slR}) \cdot \cos\gamma_1 \cdot a_o - (F_{suL} + F_{slL}) \cdot a_i \\ &-(F_{suR} + F_{slR}) \cdot \sin\gamma_1 \cdot (l_a - x) + (F_{bfR} + F_{brR}) \cdot b_o - (F_{bfL} + F_{brL}) \cdot b_i \\ &+(F_{fjR} + F_{fjL}) \cdot (l_b - x) + (F_{frR} + F_{frL}) \cdot (l + l_b - x) = 0 \end{aligned} \tag{4}$$

$$\begin{aligned} &I_{xx} \cdot \ddot{\psi} + (F_{SfL} + F_{SrL}) \cdot b_i - (F_{SfR} + F_{SrR}) \cdot b_o \\ &-(F_{fjR} + F_{fjL} + F_{frR} + F_{frL}) \cdot (z + h) - F_{suR} \sin\gamma_1 \cdot e_1 + F_{slR} \sin\gamma_1 \cdot e_2 = 0 \end{aligned} \tag{5}$$

$$I_{zzb} \cdot \ddot{\varphi}_b - (F_{suR} + F_{slR}) \cos\gamma \cdot l_o \cos\varphi_b - (F_{suR} + F_{slR}) \sin\gamma \cdot l_o \sin\varphi_b = 0 \tag{6}$$

where m, I_{yy}, I_{xx} and I_{zzb} are the mass of the vehicle body, the moment of inertia of the vehicle body about the y-axis, the moment of inertia of the vehicle body about the x-axis, the moment of inertia of the vehicle body about z-axis at the point of impact and the moment of inertia of the rotation part of the bumper about the z-axis at the point of impact, respectively. $\ddot{x}$ and $\ddot{z}$ are the acceleration of the vehicle body in longitudinal direction and the acceleration of the vehicle body in the vertical direction, respectively. $\ddot{\theta}$, $\ddot{\varphi}$, $\ddot{\psi}$ and $\ddot{\phi}_b$ are the rotational pitching, yawing, rolling accelerations of the vehicle body and rotational acceleration of the rotation part of the bumper, respectively. x and z are the vehicle body longitudinal and vertical displacements, respectively. As shown in Figure 9, φ, φ_b, γ and γ_1 represent the vehicle body yaw angle, the rotational part of the bumper angle, the angle between the front-end right springs and x-axis and the difference

angle between φ and γ, respectively. F_s, F_b, F_S and F_f are the front-end non-linear spring forces, the braking forces, the vehicle suspension forces and the friction forces between the tyres and the road due to vehicle yawing, respectively.

Figure 6 Illustration drawing of the front-end deformation due to vehicle pitching

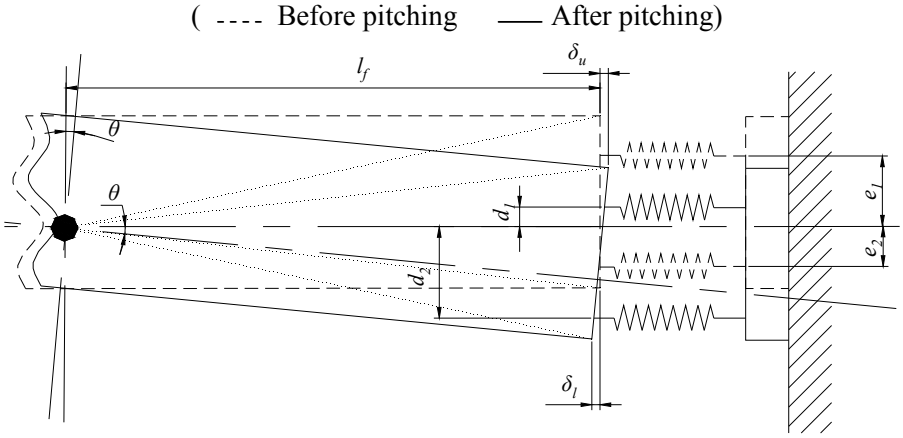

Figure 7 The behaviour of the right and left front-end springs while crashing with finite element model (see online version for colours)

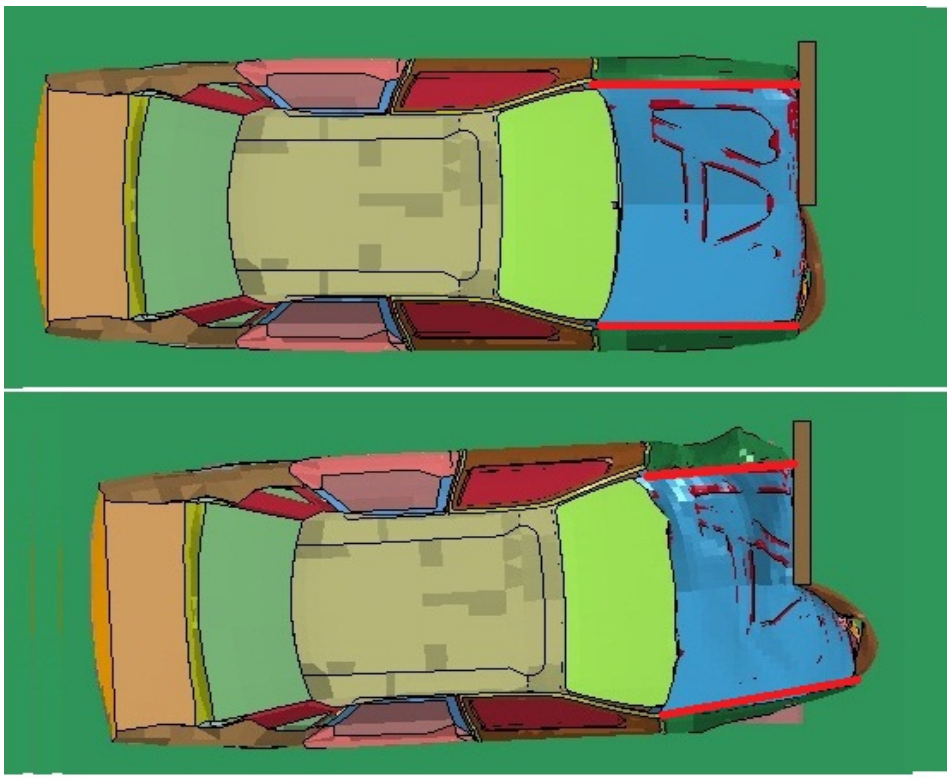

Figure 8 Illustration drawing of the front-end deformation due to vehicle yawing (see online version for colours)

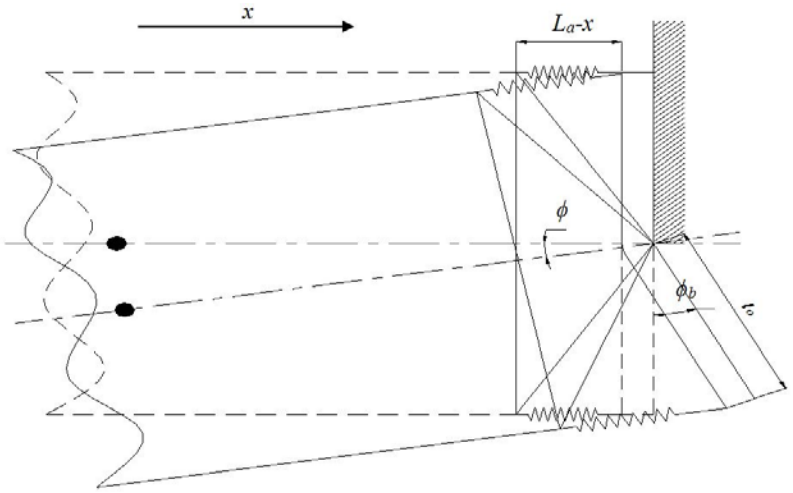

Figure 9 Simplification of Figure 4b its free-body diagram (see online version for colours)

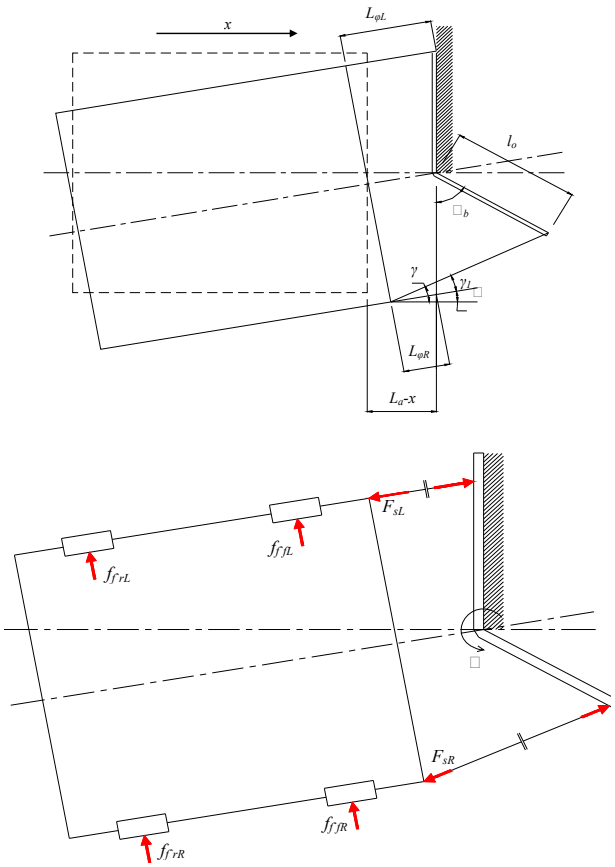

The front-end springs' location is represented by the subscripts u_R, u_L, l_R and l_L which denote upper right spring, upper left spring, lower right spring and lower left spring, respectively. The vehicle wheel location is represented by the subscripts f_R, f_L, r_R and r_L which denote front right wheel, front left wheel, rear right wheel and rear left wheel, respectively. l_a, l_b, l_o, e_1 and e_2 represent the length of the front-end springs, distance between the bumper and the centre of front wheels, distance between the point of impact and the end of rotational part of the bumper, the distance between the CG and front-end upper springs and the CG and front-end lower springs, respectively. d_1 and d_2 represent the distance between the CG and the upper springs force and the CG and the lower springs force, respectively, and can be calculated using Figure 6 as:

$$d_1 = \sqrt{l_f^2 + e_1^2} \cdot \sin\left(\tan^{-1}\left(\frac{e_1}{l_f}\right) - \theta\right) \tag{7}$$

$$d_2 = \sqrt{l_f^2 + e_2^2} \cdot \sin\left(\tan^{-1}\left(\frac{e_2}{l_f}\right) + \theta\right) \tag{8}$$

and angles γ and γ_1 can be calculated as, shown in Figure 9:

$$\gamma = \tan^{-1}\left(\frac{l_o - l_o \cos\varphi_b}{l_o \cdot \sin\varphi_b + l_{\varphi R} \cdot \cos\varphi}\right) \tag{9}$$

$$l_{\varphi R} = \frac{(l_a - x) - a_o \sin\varphi}{\cos\varphi} \tag{10}$$

$$\gamma_1 = \gamma - \varphi \tag{11}$$

4 Model forces

In this simulation the braking force F_b for each wheel can be calculated as:

$$F_{bk} = \mu(\lambda) \cdot F_{zk} \tag{12}$$

where μ is the friction coefficient between the tyre and the road, λ is the tyre–slip ratio and F_z is the vertical normal forces of the tyres. The subscript k indicates the wheel location (f_R is front right wheel, f_L is front left wheel, r_R is rear right wheel and r_L is rear left wheel). The slip ratio λ can be estimated using the wheel model discussed by Ting and Lin (2004). Relating to the values of λ, the ABS controller turns the brake on/off to sustain μ at its maximum values; therefore, the maximum braking force can be obtained. The vertical forces F_{zk} at each wheel can be written as follows:

$$F_{zfR} = m \cdot g \cdot \frac{l_r}{l} + F_{SfR} \tag{13}$$

$$F_{zfL} = m \cdot g \cdot \frac{l_r}{l} + F_{SfL} \tag{14}$$

$$F_{zrR} = m \cdot g \cdot \frac{l_f}{l} + F_{SrR} \tag{15}$$

$$F_{zrL} = m \cdot g \cdot \frac{l_f}{l} + F_{SrL} \tag{16}$$

The AS force elements are taken to be 1000 N in the upward direction with the maximum suspension travel limit of 100 mm taking into consideration the response time of the AS system (Ting and Lin, 2004). The suspension forces can also be written as follows:

$$F_{SfR} = k_{SfR}\left(z - l_f \cdot \sin\theta - b_o \cdot \psi\right) + c_{fR}\left(\dot{z} - l_f \cdot \dot{\theta} \cdot \cos\theta - b_o \cdot \dot{\psi}\right) - u_{fR} \tag{17}$$

$$F_{Sfl} = k_{SfL}\left(z - l_f \cdot \sin\theta + b_i \cdot \psi\right) + c_{fL}\left(\dot{z} - l_f \cdot \dot{\theta} \cdot \cos\theta + b_i \cdot \dot{\psi}\right) - u_{fL} \tag{18}$$

$$F_{SrR} = k_{SrR}\left(z + l_r \cdot \sin\theta - b_o \cdot \psi\right) + c_{rR}\left(\dot{z} + l_r \cdot \dot{\theta} \cdot \cos\theta - b_o \cdot \dot{\psi}\right) - u_{rR} \tag{19}$$

$$F_{SrL} = k_{SrL}\left(z + l_r \cdot \sin\theta + b_i \cdot \psi\right) + c_{rL}\left(\dot{z} + l_r \cdot \dot{\theta} \cdot \cos\theta + b_i \cdot \dot{\psi}\right) - u_{rL} \tag{20}$$

where k_S, c and u represent the stiffness of the suspension springs, damping of the suspension coefficients and active suspension force elements, respectively. θ and ψ are the vehicle body pitching and rolling angels, respectively. $\dot{z}$, $\dot{\theta}$ and $\dot{\psi}$ represent the vehicle body vertical velocity, pitching velocity and rolling velocity, respectively.

To simulate the upper and lower members of the vehicle front structure, multi-stage piecewise linear force-deformation spring characteristics are considered, as shown in Figure 10. The non-linear springs used in the multi-body model are taken to generate the n stage piecewise spring's characteristics, as shown in Figure 11. The forces of the non-linear springs shown in Figure 10 are defined using piecewise functions in the displacement domain as follows:

$$F_{si} = k_{sij}\delta_i + F_{ij} \tag{21}$$

where k_s and δ represent the stiffness and the deflection of the front-end spring, respectively. The subscript i indicates the spring location (u_R is upper right spring, u_L is upper left spring, l_R is lower right spring and l_L is lower left spring) and the subscript j indicates different stages of the force-deformation characteristics as shown in Figure 10. The stiffness of the spring k_s and the force elements F_{ij} vary according to the different stages of the deflection δ and can be defined as follows:

$$k_{sij} = k_{si1}, \qquad F_{ij} = 0, \qquad 0 \le \delta < \delta_{i1} \tag{22}$$

$$k_{sij} = k_{si2}, \qquad F_{ij} = (k_{si1} - k_{si2})\delta_{i1} \qquad \delta_{i1} \le \delta < \delta_{i2} \tag{23}$$

$$k_{sij} = k_{si3}, \qquad F_{ij} = \left(k_{si1} - k_{si2}\right)\delta_{i1} + \left(k_{si2} - k_{si3}\right)\delta_{i2} \qquad \delta_{i2} \le \delta < \delta_{i3} \tag{24}$$

$$\begin{aligned} k_{sij} = k_{\sin}, \qquad F_{ij} &= \left(k_{si1} - k_{si2}\right)\delta_{i1} + \left(k_{si2} - k_{si3}\right)\delta_{i2} + \ldots \\ &+ \left(k_{si(n-1)} - k_{\sin}\right)\delta_{i(n-1)} \qquad \delta \ge \delta_{(n-1)} \end{aligned} \tag{25}$$

where the deformations of the front-end springs δ_i can be calculated using Figures 6 and 9 as:

$$\delta_{uR} = x + \delta_{\theta uR} + \delta_{\varphi uR} - \delta_b \tag{26}$$

$$\delta_{uL} = x + \delta_{\theta uL} - \delta_{\varphi uL} \tag{27}$$

$$\delta_{lR} = x - \delta_{\theta lR} + \delta_{\varphi lR} - \delta_b \tag{28}$$

$$\delta_{lL} = x - \delta_{\theta lL} - \delta_{\varphi lL} \tag{29}$$

where δ_θ, δ_φ and δ_b represent deflection of the front end due to pitching, yawing and the bumper's rotation, respectively, and can be calculated as:

$$\delta_{\theta uR} = \delta_{\theta uL} = \sqrt{l_f^2 + e_1^2} \cdot \cos\left(\tan^{-1}\left(\frac{e_1}{l_f}\right) - \theta\right) - l_f \tag{30}$$

$$\delta_{\theta lR} = \delta_{\theta lL} = l_f - \left[\sqrt{l_f^2 + e_2^2} \cdot \cos\left(\tan^{-1}\left(\frac{e_2}{l_f}\right) + \theta\right)\right] \tag{31}$$

$$\delta_{\varphi uR} = \delta_{\varphi lR} = (l_a - x) - l_{\varphi R} \tag{32}$$

$$\delta_{\varphi uL} = \delta_{\varphi lL} = l_{\varphi l} - (l_a - x) \tag{33}$$

$$l_{\varphi L} = \frac{(l_a - x) + a_i \sin\varphi}{\cos\varphi} \tag{34}$$

$$\delta_b = \sqrt{\left(l_o - l_o \cos\varphi_1\right)^2 + \left(l_o \cdot \sin\varphi_1 + l_{\varphi R} \cdot \cos\varphi\right)^2} - l_{\varphi R} \tag{35}$$

Figure 10 General piecewise force-deformation characteristics (see online version for colours)

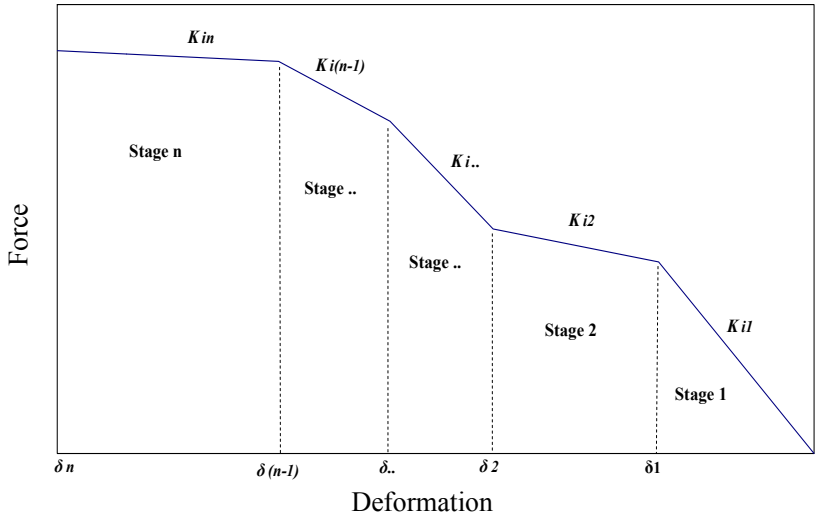

Figure 11 Force deformation characteristics for upper and lower rails (see online version for colours)

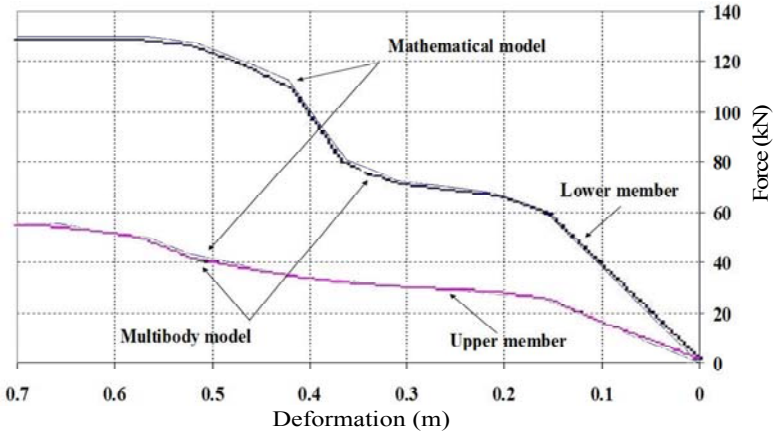

5 Comparison between the model, real data and other model results

In this section, comparisons between the mathematical model, real test data and former multi-body model are established. The main reason for these analyses is to ensure that the mathematical model is reliable and can be used accurately in this study. In the real crash test, the vehicle was in free-rolling mode with an impact speed of 16.1 m/s; therefore, the same conditions are used in the mathematical model simulation. The comparison of the mathematical model, ADAMS multi-body model and real test results from (TRL, 1995), are depicted in Figures 12–14. ADAMS model incorporates a fully independent suspension system, connecting Fiala tyre models to the rigid main body of the vehicle. The crash structure of the vehicle consists of four non-linear spring damper sets connecting rigid cross members to the rigid cabin of the vehicle, in which two represent the lower structure and the main longitudinal chassis members and other two represent the upper members of the structure (Hogan, 2008). The lower initial speed of 15.1 m/s at the moment of the impact of the ADAMS model as shown in Figure 12 is due to the effect of rolling resistance prior to impact (Hogan, 2008), while the initial speed of the mathematical model is adapted to be the same as the actual test impact speed. However, the post-impact velocity curve of the mathematical model is in a good correlation with both real test and ADAMS model results.

In the vehicle body deceleration results shown in Figure 13, a high correlation between the mathematical model and ADAMS model and the mean results of the real test is observed. The sudden reduction of the vehicle deceleration at the end of collision at the mathematical model and ADAMS results is due to the deactivation of the spring forces at this point (there is no recoil of the springs). Although the mathematical model predicted a slightly higher value than ADAMS results, the mean value of deceleration is approximately the same as that of the actual results. The deformation of the front-end structure is illustrated in Figure 14, and a slightly lower value of the maximum deformation appeared in the mathematical model. This may be due to mass differences or other assumed parameters. However, the trend in the three cases is approximately the same with small differences in the maximum deformations.

Figure 12 Velocity of the vehicle body (see online version for colours)

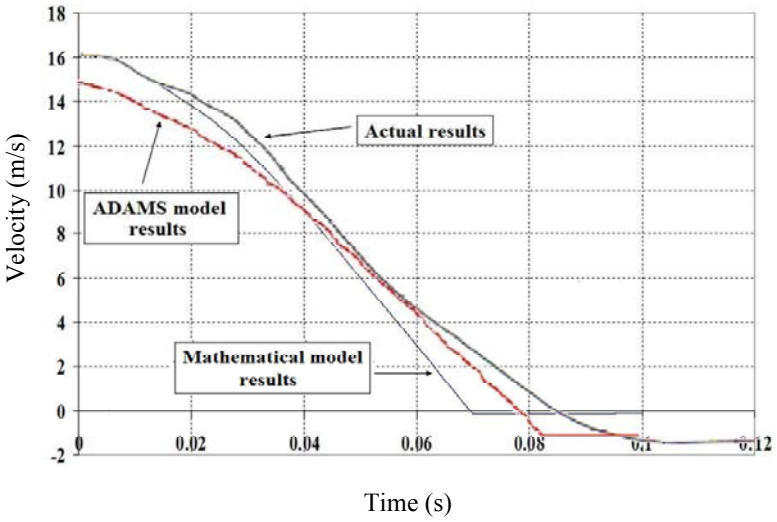

Figure 13 Deceleration of the vehicle body (see online version for colours)

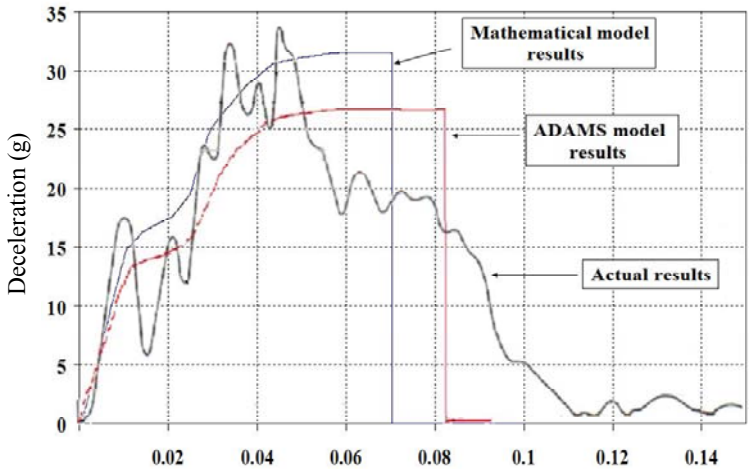

Figures 15 and 16 show the comparison between the mathematical model results and ADAMS results for vehicle yaw velocity and acceleration. In Figure 15 the vehicle velocities are almost the same in both models until reaching the maximum values (at the end of crash). Vehicle yaw velocity after the end of crash is depending on the maximum vehicle pitch angle and it will be described in later section of the paper. While the maximum vehicle yaw acceleration is slightly higher in ADAMS model results than the mathematical model results, a good correlation between both results is noted.

Figure 14 Deformation of the front-end structure (see online version for colours)

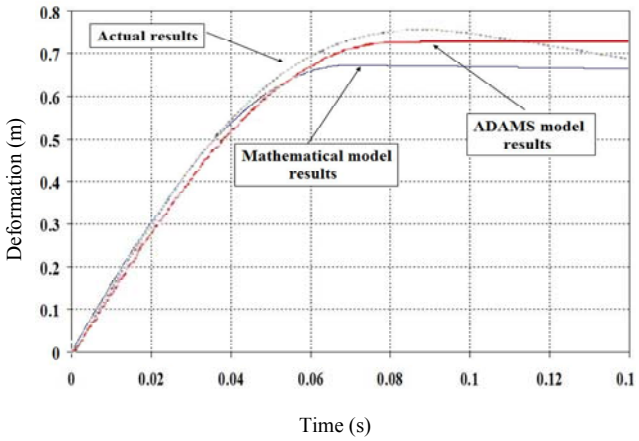

Figure 15 Yaw velocity of the vehicle body

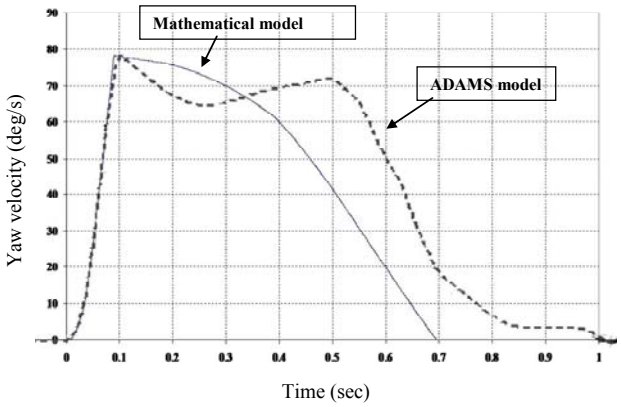

Figure 16 Yaw acceleration of the vehicle body

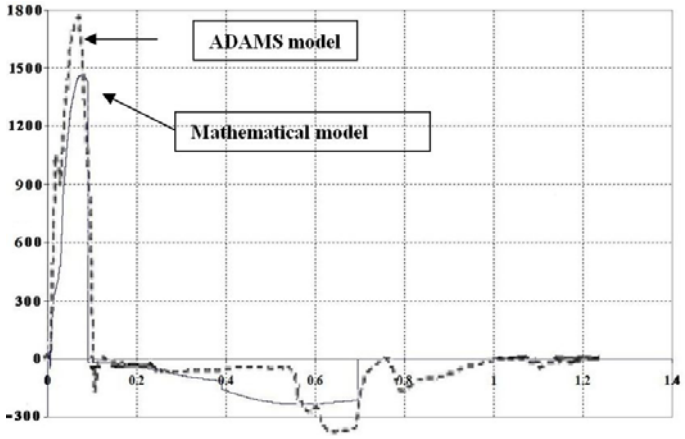

6 Crash scenarios simulation

Different crash scenarios have been simulated with different cases of VDCS to obtain the optimum set of control systems in impending collision. In this study, the optimisation method depends on the selection of a best element from some set of available alternatives. The vehicle dynamics/crash mathematical model as shown in Figure 1 has been developed and used to conduct such a study. The model is validated as described in the previous section and proven to be in good conformity with the ADAMS model and the experimental results provided by TRL data. Table 1 introduces the different cases of active control systems which are used in this study. In addition, the effect of suspension damping is taken into consideration, and three different damping coefficients are used. Table 2 shows the values of the different parameters which are used in the simulations.

Table 1 Numerical study matrix

Case number		*Description*	*Control Parameter*
1	Free rolling	Vehicle impacted the barrier without any activated control systems	Non
2	ABS	ABS is applied	Anti-Lock braking control
3	ABS + DYC system	DYC is applied along with ABS	Anti-Lock braking control + Direct yaw control
4	Anti Pitch Control (with different three AS force elements)	Anti-pitch control system is applied using the AS components and ABS is also applied	Anti-Lock braking control + Active suspension control
5	Under Pitch Technique (with different three AS force elements)	AS is applied to front wheels in upward direction while applied to rear wheels in downward direction to give the vehicle negative pitching angle before crash and ABS is also applied	Anti-Lock braking control + Active suspension control

In all cases, the deformation of the impacted side (left side) of the front-end structure and deceleration of the vehicle body as well as yaw angle, yaw velocity and yaw acceleration are determined. While ADAS detected that the crash would be unavoidable 1.5 s prior to the impact (Jansson et al., 2002), VDCS will be applied in this short time preceding the impact. The initial velocity is different in each case (depending on each case of the active control systems) and all velocities will be the same (55 km/h) after 1.5 s when the vehicle reaches the barrier.

In the following results the normal damping coefficient c_2 and the AS force f_{a1} are used. Figure 17 shows the impacted side of the front-end structure's deformation-time histories of all cases; while Figure 18 captures the maximum deformation value of each case. Small differences in the maximum deformation of the vehicle's impacted side are found in the different six cases; however, the minimum deformation is obtained in the cases 2, 4 and 5 with almost the same values. In these three cases a reduction of about 20 mm is obtained compared with free-rolling case. On the other hand, case 3 (ABS + DYC) produced a higher deformation with a total reduction of about 15 mm. Related to the study discussed by Ting and Lin (2004), when the AS control system is integrated with the ABS, the braking force can be increased due to the increase of vertical load, and the minimum stopping distance can be obtained. In this study, the application of the AS control system (cases 4 and 5) helps reduce the maximum deformation of the front-end structure as shown in Figure 18. As part of this analysis, it is also found that the suspension damping coefficient does not affect vehicle body front-end deformation.

Table 2 The values of the different parameters which are used in the simulations

Parameter	*Value*
m	1200 kg
I_{yy}	1490 kg.m^2
I_{xx}	350 kg.m^2
I_{zz}	1750 kg.m^2
I_{bzz}	40 kg.m^2
$k_{SfR} = k_{SfL}$	18.25 kN/m
$k_{SrR} = k_{SrL}$	13.75 kN/m
l_f	1.185 m
l_r	1.58 m
h	0.452 m
l_a	1.2 m
l_b	0.85 m
$b_i = b_o$	0.8 m
Damping coefficients *c1*, *c2* and *c3* represent different cases of low, normal and high suspension damping, respectively, and the following values are used	
$c_{fR1} = c_{fL1}$	500 N.s/m
$c_{rR1} = c_{rL1}$	425 N.s/m
$c_{fR2} = c_{fL2}$	1100 N.s/m
$c_{rR3} = c_{rL3}$	900 N.s/m
$c_{fR3} = c_{fL3}$	1575 N.s/m
$c_{rR2} = c_{rL2}$	1350 N.s/m
The different three values of the active force element for each wheel are selected as follows	
f_{a3}	1000 N
f_{a2}	2000 N
f_{a1}	3000 N

Figure 17 Deformation of the vehicle front-end for all cases (see online version for colours)

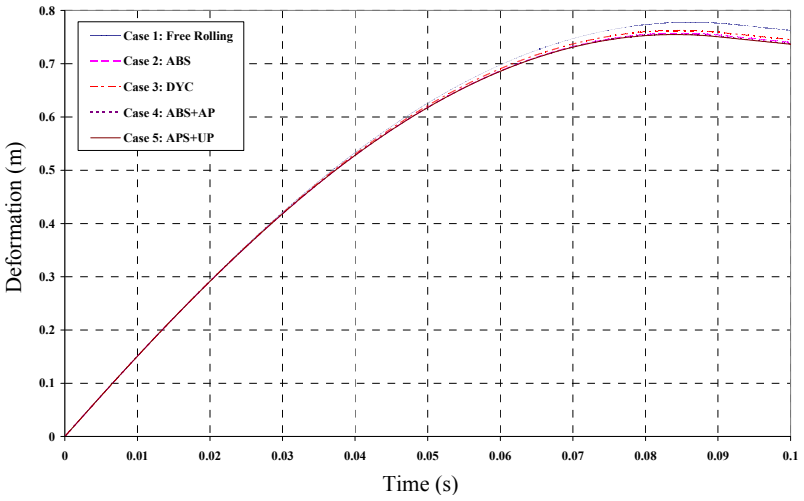

Figure 18 Maximum values of the vehicle front-end deformations (see online version for colours)

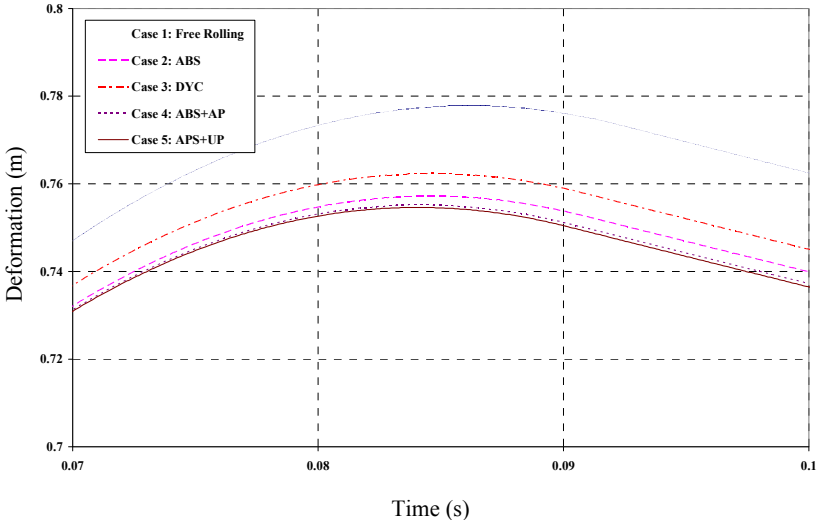

Vehicle body deceleration–time histories for all cases are depicted in Figure 19 and no significant difference in trends or values can be found. However, in cases 2, 4 and 5, very small higher values of the maximum deceleration are observed compared with cases 1 and 3. These higher values are due to the application of braking force, which does not exist in a free-rolling case and is deactivated in DYC case to reduce the yawing moment. The fast reduction in the vehicle body deceleration (arrow 1 in Figure 19) occurs when the front left wheel reaches the barrier and its braking effect is ended. Also, at the end of collision the vehicle is stopped and starts moving in the opposite direction; meanwhile the braking force also change its direction, and the deceleration is suddenly decreased, as shown in Figure 19 (arrow 2).

Figure 19 Deceleration of the vehicle body for all cases (see online version for colours)

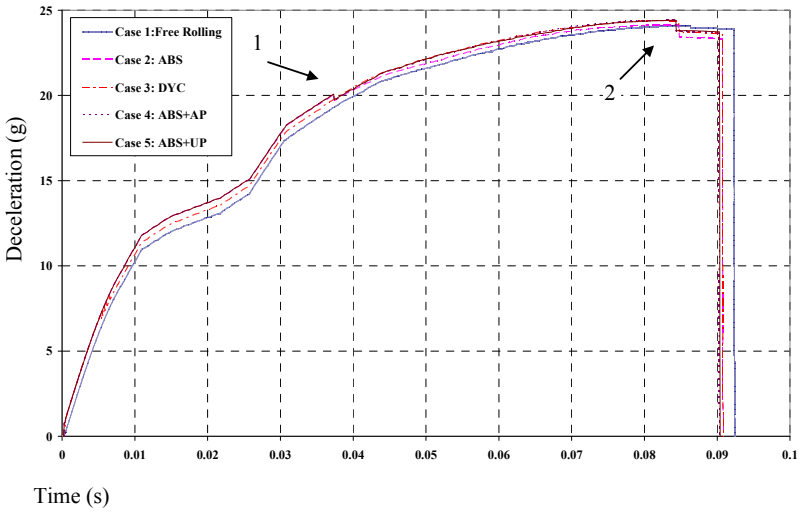

6.1 Yawing analysis

In the offset collision, only one side of the vehicle is impacted, which creates a high difference between the right and left front-end springs' forces, and that is the main source of the yaw moment that makes the vehicle body rotate around the *z*-axis. Figure 20 shows the vehicle yaw velocity–time histories for all cases with the same normal vehicle suspension damping coefficient c_2. Vehicle yaw velocity is equal to zero before crash then it is changed in three different stages: first, it is increased rapidly to reach its maximum value; second it is decreased slowly to reach a specific value; and third it is decreased gradually to reach zero value. In the first stage, the rapid increase in the yaw velocity is due to the high acceleration (see Figure 21) caused by the one side-impacted spring. At the end of collision, the rear wheels have already left the ground due to the vehicle pitching (Elkady et al., 2011), and the vehicle is now controlled by only the front wheels. So, in the second stage, the decreasing in the vehicle's yaw velocity is due to the friction force between the front tyres and the ground. Stage 3 begins when the rear wheel starts contact the ground which generates yaw moment in the opposite direction causing a reduction of the vehicle yawing velocity with a higher rate than the decreasing of velocity rate in the second stage.

Figure 20 Yaw velocity of the vehicle body for all cases (see online version for colours)

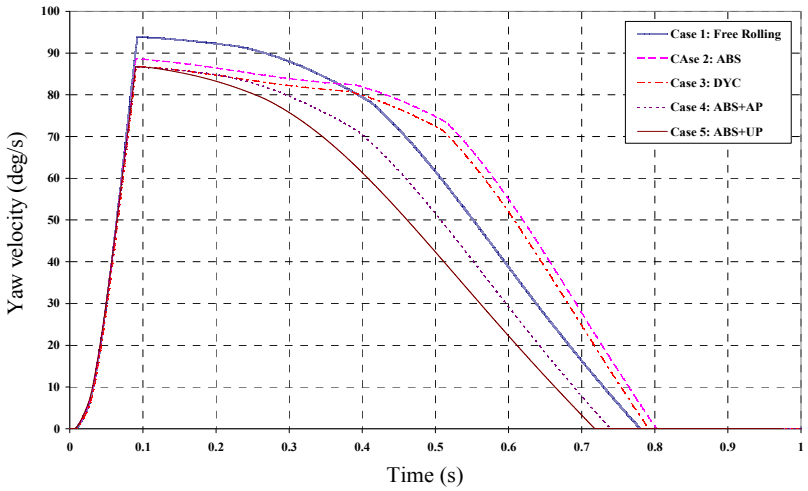

Because of the maximum vehicle front-end deformation is observed in case 1 (free rolling), as shown in Figure 18, the greatest peak of yaw velocity appears in the same case, as shown in Figure 20. The maximum yaw velocities are approximately the same for all other cases, with a slight increase in the case of applying only the ABS. The period of the second stage is different for each case and is mainly depend on pitching angle.

Vehicle body yaw acceleration–time histories are depicted in Figure 21. Maximum yaw acceleration is discovered in case 1 (free rolling), and yaw acceleration for the other cases is approximately the same with a slight increase in case 2 (ABS). At the end of collision the vehicle is controlled by only the front wheels, as mentioned before, which try to hinder the yawing motion, and the negative acceleration is shown with different small values related to each case. These negative values of the vehicle yaw acceleration are increased slowly with time; then they are increased rapidly when the rear wheels reach the ground.

Figure 21 Yaw acceleration of the vehicle body for all cases (see online version for colours)

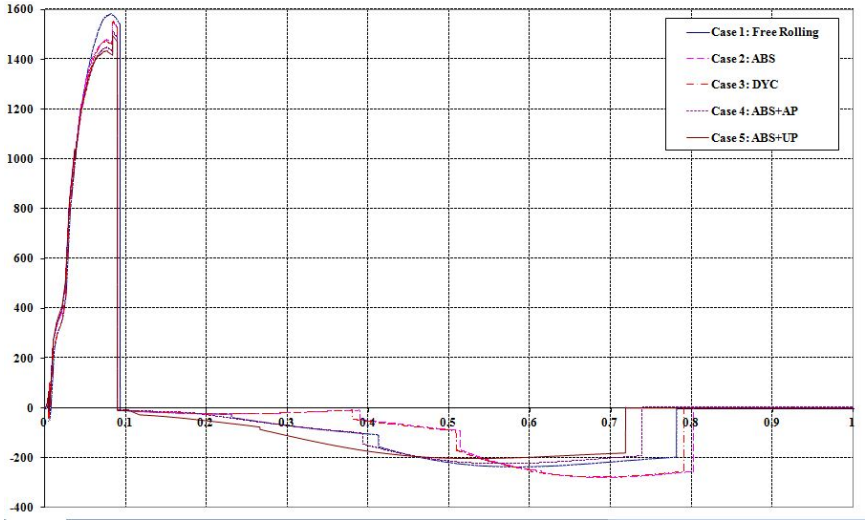

Figure 22 shows the vehicle body yaw angle–time histories for all cases. It found that the maximum yaw angle of 49.3° is noticed in case 2 (ABS) while the minimum yaw angle of 36.8° is noticed in case 5 (ABS + UP). The maximum value of the vehicle yaw angle depends on the maximum yaw acceleration and the vehicle pitch angle for each case. The reduction of about 12.5° (25%) is obtained when the UP control is applied along with ABS, compared with only ABS is applied. As described in Table 1, the UP technique is used to make the vehicle pitching up for few degrees before crash. Reducing the maximum vehicle body yaw angle reduces the risk of the car side-impact by any obstacles on the road. From this yawing analysis it can be said that the best set of the vehicle dynamic control is to apply case 5 (ABS + UP), because the minimum yaw angle and acceleration are obtained in this case.

Figure 22 Yaw angle of the vehicle body for all cases (see online version for colours)

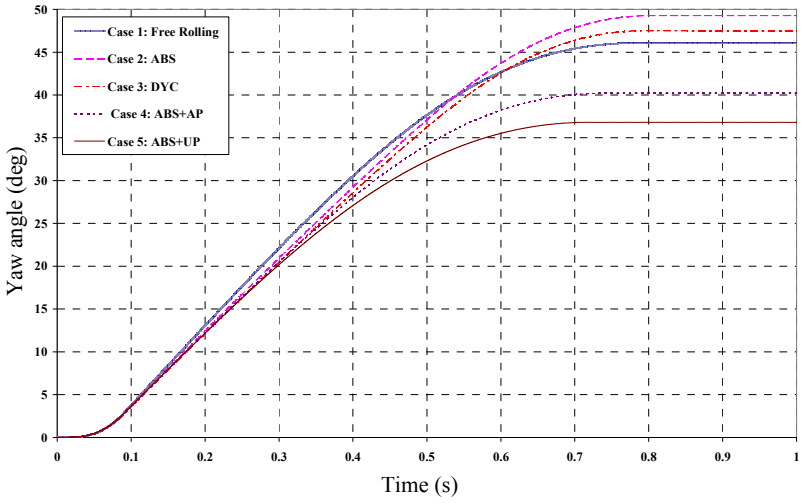

6.2 Effect of different AS force elements on vehicle yawing

AS control system is used to perform the AP control and UP condition, cases 4 and 5 in this study. Three different values of AS (f_{a1}, f_{a2} and f_{a3}) force are selected to study their effect on vehicle yawing during and post-impact. Figure 23 depicts the vehicle yawing velocities for cases 4 and 5 with the three different values of AS. It is demonstrated from Figure 23 that a reduction in vehicle peak yawing velocity is observed in case 4, f_{a3} and case 5, f_{a2}, while the lowest peak velocity is shown in cases 4, f_{a2} and 5, f_{a3}.

Figure 23 Vehicle yaw velocity for cases (4 and 5) with different values of active suspension force element (see online version for colours)

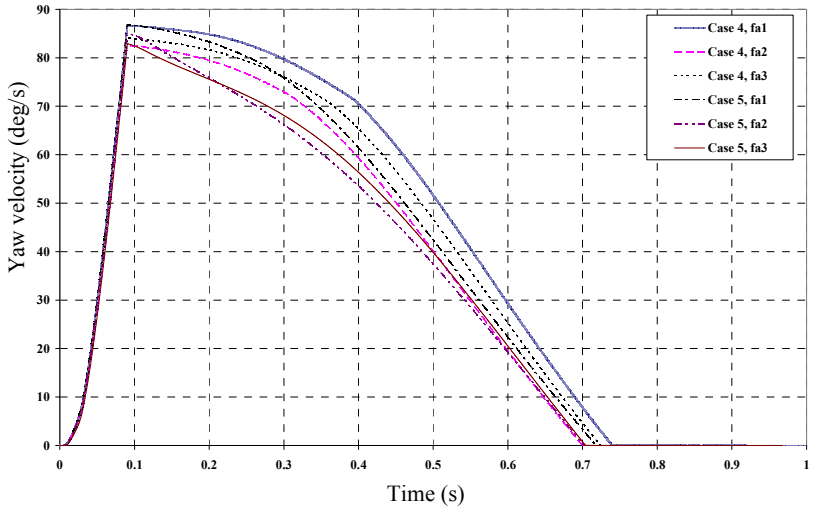

Figure 24 shows the vehicle yawing acceleration for the same cases, while the differences between the results of the different cases are very small, the highest yaw acceleration is observed in case 5, f_{a3} and the lowest acceleration is found in cases 4, f_{a2} and case 5, f_{a2}. The yawing angle has been reduced to 33° in case 5, f_{a2} and 33.6° in case 5, f_{a2} as shown in Figure 25. From this analysis it can be confirmed that the relation between the AS force and the yawing angle, velocity and acceleration is not linear. When the AS force is increased, the vehicle pitching acceleration is also increased, and that causes an increase in the vehicle pitching as well. That explains why in case 5, f_{a2} and case 4, f_{a2} the yawing angle is smaller than in case 5, f_{a3} and case 4, f_{a2}, respectively. To obtain the optimum AS force that helps obtain the minimum yaw angle, the relation between the AS force and yaw angle should be studied separately.

6.3 Effect of damping coefficient on vehicle crash

Three different values of the damping coefficient for each case of VDCS are used to study the effect of the vehicle suspension damping coefficient on vehicle crash. The effect of damping coefficient is the same for all cases, with slightly different values, so case 5 with AS force f_{a2} (optimum case in this study) is used to show that effect. It is found that there are no changes in the vehicle front-end deformation or vehicle deceleration with the different damping coefficients as mentioned before, however, the vehicle yawing behaviour is affected by the vehicle suspension damping coefficient.

Figure 24 Vehicle yaw acceleration for cases (4 and 5) with different values of active suspension force element (see online version for colours)

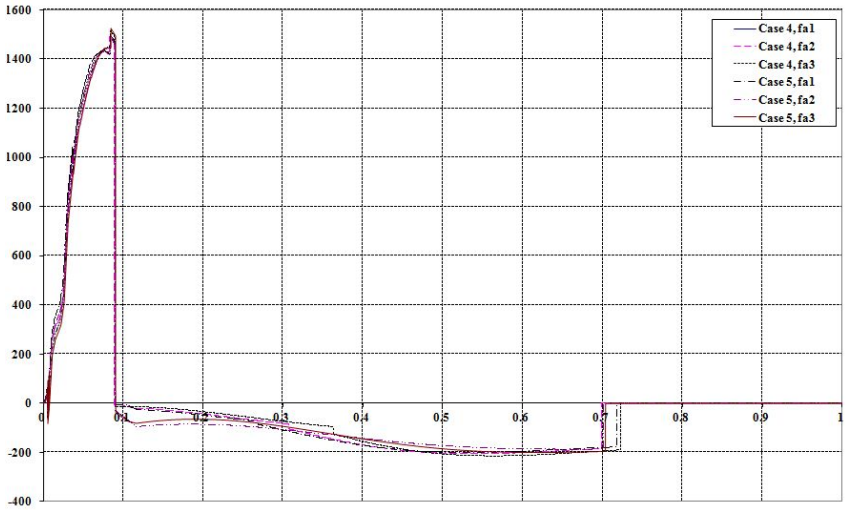

Figure 25 Vehicle yaw angle for cases (4 and 5) with different values of active suspension force element (see online version for colours)

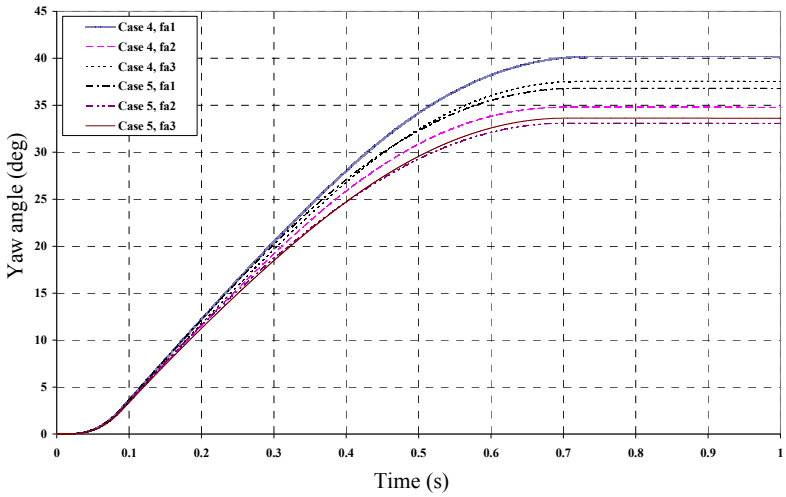

Figure 26 shows the vehicle yaw velocity–time histories for case 5, f_{a2} (ABS + UP with AS force of 2000 N) with the different three values of the vehicle suspension damping coefficients. The damping coefficient has an effect on the vehicle maximum yaw velocity; it is found that when the damping coefficient increases, the vehicle yaw velocity decreases. However, it cannot be proven that this is a linear relationship; it also needs the creation of an accurate relation curve. The period when the rear tyres leave the ground is also affected by the vehicle suspension damping coefficient and it is reduced when the damping coefficient is increased. Higher damping coefficient helps reduce the vehicle pitching, and that is the main reason for reducing the period when the vehicle rear wheels

leave the ground. The vehicle yaw acceleration–time is also depicted in Figure 27 and it is found that there is no significant effect of the vehicle suspension damping coefficient on the vehicle yaw acceleration. However, the minimum peak value of yaw acceleration is observed in case 5, f_{a2}, c_3. The vehicle yaw angle is also decreased when the damping coefficient is increased, as shown in Figure 28. A reduction of about 7° of the vehicle yaw angle can be obtained when the damping coefficient is changed from c_1 to c_3, and that may help reduce the risk of the car colliding with any other bodies on the road during its rotation.

Figure 26 Vehicle yaw velocity for case (5) with active suspension force of 2000 N (see online version for colours)

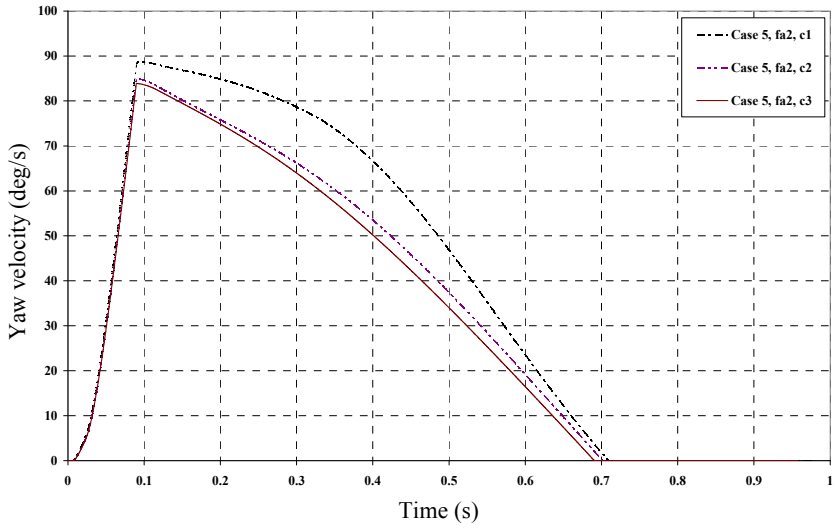

Figure 27 Vehicle yaw acceleration for case (5) with active suspension force of 2000 N (see online version for colours)

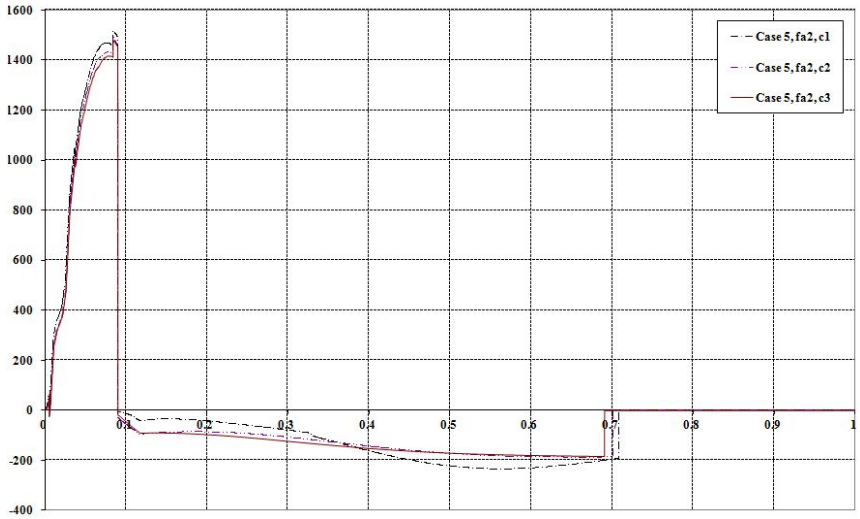

Figure 28 Vehicle yaw angle for case (5) with active suspension force of 2000 N (see online version for colours)

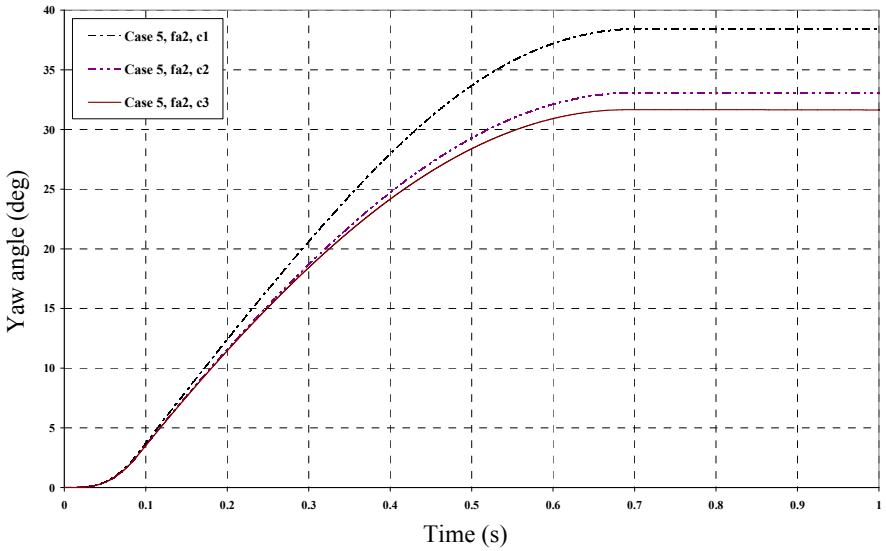

7 Conclusion

This paper has presented the (6-DOF) vehicle dynamics/crash mathematical model in order to investigate the effect of the VDCS on vehicle-to-barrier collision in offset crash scenarios. In this study, a comparison of five different VDCS scenarios has been provided to obtain the best set of VDCS in impending collision. The deformation of the impacted side of the vehicle front-end structure, the vehicle body deceleration, yaw angle, yaw velocity and yaw acceleration have been determined. It is demonstrated that the mathematical model is valid, reliable and could be used in many other crash scenarios. This study proves that the minimum impacted side of the front-end structure deformation is obtained when the ABS is applied along with UP condition, which leads to a reduction in the risk of the occupant compartment being intruded. In addition, it is shown that the minimum reduction of the vehicle body yaw angle, velocity and acceleration can be obtained if the under-pitch control is applied alongside the ABS. The effect of AS force element is discussed and it is seen that the relation between the AS force and vehicle yaw behaviour is not linear. The effect of the vehicle suspension damping coefficient is also considered and it is found that, when the damping coefficient is increased, the vehicle body yaw angle is decreased. This reduction in the maximum vehicle yaw angle helps reduce the risk of the car being side-impacted by any obstacles on the road. This study showed that the optimum set of the VDCS in impending collision for offset crash scenarios is to apply the under-pitch control alongside the ABS in order to get the benefit of reducing front-end deformation and maximum yaw angle.

Acknowledgements

The authors would like to thank the Egyptian Government and the Faculty of Engineering, Ain Shams University for supporting this research. We also acknowledge with sadness, the contribution of Prof. Dave Crolla who has passed away during the period of this research.

References

Alleyne, A. (1997) 'Improved vehicle performance using combined suspension and braking forces', *Vehicle System Dynamics*, Vol. 27, pp.235–265.

Elkady, M., Elmarakbi, A. and Crolla, D. (2011) 'A study on vehicle dynamic control systems and their influence on vehicle collisions improvement', *IEEE Intelligent Transportation Systems Society Conference*, Washington, DC, USA.

Elmarakbi, A. and Zu, J. (2004) 'Dynamic analysis of smart structures for vehicle-to vehicle frontal collision alleviation', *Transaction of Society of Automotive Engineers of Japan*, Vol. 35, pp.151–156.

Emori, R.I. (1968) 'Analytical approach to automobile collisions', *SAE World Congress & Exhibition*, Warrendale, USA.

Gietelink, O., Ploeg, J., De Schutter, B. and Verhaegen, M. (2006) 'Development of advanced driver assistance systems with vehicle hardware-in-the-loop simulations', *Vehicle System Dynamics*, Vol. 44, No. 7, pp.569–590.

Hogan, I. (2008) *The Development of a Vehicle Collision Mitigation Control System through Multibody Modelling*, FISITA World Automotive Congress, Munich, Germany.

Jansson, J., Gustafsson, F. and Johansson, J. (2002) *Decision Making for Collision Avoidance Systems*, SAE World Congress & Exhibition, Detroit, MI, USA.

Kamal, M.M. (1970) *Analysis and Simulation of Vehicle to Barrier Impact*, SAE World Congress & Exhibition, Detroit, MI, USA.

Khattab, A. (2010) *Investigation of an Adaptable Crash Energy Management System to Enhance Vehicle Crashworthiness*, PhD Thesis, the Department of Mechanical and Industrial Engineering, Concordia University, Canada.

Kim, H.S. (2002) 'New extruded multi-cell aluminum profile for maximum crash energy absorption and weight efficiency', *Thin-Walled Structures*, Vol. 40, pp.311–327.

Mastandrea, M. and Vangi, D. (2005) 'Influence of braking force in low-speed vehicle collisions', *Proceedings IMechE*, Vol. 219, pp.151–164.

Schoeneburg, R. and Breitling, T. (2005) 'Enhancement of active & passive safety by future pre-safe systems', *Proceedings of the 19th ESV Conference*, Washington, DC, USA.

Tamura, M., Inoue, H., Watanabe, T. and Maruko, N. (2001) *Research on a Brake Assist System with a Preview Function*, SAE World Congress, Detroit, MI, USA.

Ting, W.E. and Lin, J.S. (2004) 'Nonlinear control design of anti-lock braking systems combined with active suspensions', *5th Asian Control Conference*, Melbourne, Australia.

TRL (Real Crash Test Data) (1995) *Creating the Future of Transport*. Available online at: http://www.trl.co.uk

Witteman, W.J. (1999) *Improved Vehicle Crashworthiness Design by Control of the Energy Absorption for Different Collision Situations*, PhD Thesis, Eindhoven University of Technology, Eindhoven, the Netherlands.

Witteman, W.J. and Kriens, R.F.C. (1998) 'Modeling of an innovative frontal car structure: similar deceleration curves at full overlap, 40 per cent offset and 30 degrees collisions', *16th ESV Conference*, Windsor, Canada.